Sensors and Materials, Vol. 36, No. 3 (2024) 1093–1103
MYU Tokyo

S & M 3583

Exploring the Influence of Copper Chemical Displacement Duration on Nonvolatile Oxide-based Resistive Memory Device Characteristics

Chu-En Lin,[1] Bo-Qin Yu,[1] Yi-Ching Cheng,[1] Hsin-Chiang You,[1] I-Nan Chang,[2] Jung-Chih Lin,[3,4] and Chi-Chang Wu[1*]

[1]Department of Electronic Engineering, National Chin-Yi University of Technology, Taichung 411030, Taiwan
[2]Department of Electronics Engineering, Feng Chia University, Taichung 40724, Taiwan
[3]Department of Integrated Chinese and Western Medicine, Chung Shan Medical University Hospital, Taichung 402306, Taiwan
[4]School of Medicine, Chung Shan Medical University, Taichung 402306, Taiwan

(Received October 30, 2023; accepted March 1, 2024)

Keywords: resistive memory, electrochemical metallization, chemical displacing technique, copper electrode

Nonvolatile memory devices play a pivotal role within sensor systems, serving as integral components that significantly enhance the efficiency, reliability, and overall performance of these advanced technologies. In this paper, we present a nonvolatile oxide-based resistive memory device employing a chemical displacement technique (CDT) for copper thin film as the metal electrode. The utilization of CDT-Cu offers several distinct advantages, including cost-effectiveness, high selectivity, and the ability to operate at lower temperatures. Notably, the CDT-Cu film exhibits a rough surface, which proves advantageous for facilitating the formation of filament pathways in the electrochemical metallization (ECM)-type resistive random-access memory (ReRAM) device. We systematically investigated the surface roughness of CDT-Cu samples, varying chemical displacement time, to shed light on the influence of the Cu electrode on the electrical performance of the resistive memory devices. The findings indicate that devices subjected to shorter CDT times, which yields rougher surfaces, demonstrate lower operation electric fields and enhanced reliability. This is attributed to the reduced voltage requirements, effectively mitigating the impact of Joule heating during device operation.

1. Introduction

In the age of Artificial Intelligence of Things (AIOT), memory devices play a critical role in the realm of modern technology.[1–3] These memory devices, characterized by their function of retaining stored information even when power is removed, contribute to the seamless integration and functionality of sensor systems in numerous applications. One key aspect of their importance lies in data persistence, which allows sensor systems to store and recall critical information over extended periods without the risk of data loss. Moreover, nonvolatile memory devices enhance

*Corresponding author: e-mail: ccwu@ncut.edu.tw
https://doi.org/10.18494/SAM4740

ISSN 0914-4935

the robustness and versatility of sensor systems by facilitating the implementation of complex algorithms and calibration data. The ability to store calibration parameters and algorithmic instructions directly within the memory of the sensor system ensures consistent and accurate performance over time. This is particularly crucial in applications where precise measurements and reliable data interpretation are paramount, such as in medical devices, environmental monitoring, and industrial automation.

To fulfill the demands of practical applications, these memory devices must have specific characteristics such as low power consumption, ample storage capacity, high reliability, swift operation speed, and cost-effectiveness.[4–6] Currently, flash memory devices dominate the market as the most commonly utilized memory units. However, as technology continually shrinks the dimensions of these devices, they encounter challenges related to disturbance and charge storage.[7] To address these issues, various nonvolatile memory alternatives have been explored as potential replacements for flash memory. Notable candidates in this pursuit include ferroelectric random access memory (FeRAM),[8] phase-change random access memory (PCRAM),[9] magnetic random access memory (MRAM),[10] and resistive random access memory (ReRAM).[11–13]

Among these alternatives, ReRAM devices have garnered considerable attention due to their advantageous features. These devices are characterized by their straightforward structure, minimal power consumption, high compatibility with existing systems, and exceptional scalability.[14] As a result, ReRAM devices are emerging as a promising solution in the evolving landscape of memory technology.

Copper (Cu) is distinguished by a range of exceptional properties, including low resistivity, ease of deposition, and impressive electromigration characteristics. These attributes have made it a widely adopted material for interconnections in the backend processes of semiconductor manufacturing.[15] Additionally, Cu is employed in the electrochemical metallization (ECM)-type ReRAM by leveraging copper ions in redox reactions.[16] However, one notable drawback of using copper in semiconductor devices is its resistance to precise patterning via dry etching owing to the formation of nonvolatile by-products following the etching process. Although this challenge can be overcome by employing the damascene method, the applications of Cu in ReRAM devices can be complex and cumbersome.

To address these issues, in this study, we explore a chemical displacement technique (CDT) for depositing Cu thin film to displace the titanium (Ti) film. The Cu thin film is subsequently used as the electrode in ReRAM devices. The CDT method offers several advantages, including cost-effectiveness, high selectivity in displacement, the creation of discontinuous nanoparticles, and a rough surface texture. By introducing a CDT-Cu thin film, not only is the aforementioned patterning issue mitigated, but self-aligning properties are also obtained.[17]

In this investigation, we displaced the patterned titanium film with the CDT-Cu thin film, which served as the bottom electrode for the ReRAM device. We further examined the effects of CDT time on the electrical performance of oxide-based ReRAM devices.

The findings of this study indicate that the surface roughness of the CDT-Cu film increases with longer CDT time. In comparison with conventionally sputtered Cu film, the CDT-Cu film displays a notably rougher surface. This distinction is crucial as the Cu film serves as the ion

source in the ECM-type ReRAM device. The increased surface roughness of the Cu thin film has the potential to amplify the local electric field within the device. Essentially, this means that the Cu ions can be more readily stimulated when the local electric field is intensified, subsequently leading to a reduction of the SET operation voltage. Furthermore, this heightened surface roughness contributes to an effective reduction of the Joule heating effect within the switching layer, primarily attributable to the lower operating electric field. These results have a positive impact on enhancing the reliability characteristics of the CDT-Cu ReRAM device. It is important to note that the roughness of the Cu surface can be adjusted by varying the CDT time, thus offering a degree of control over this critical aspect.

2. Materials and Methods

In this study, a metal–dielectric layer–metal sandwich structure was employed to examine the electrical properties of a CDT-Cu ReRAM device. The fabrication process of the memory device is schematically depicted in Fig. 1. The initial substrate utilized was a 6-inch p-type (100) silicon wafer. Before depositing the thin film, the wafer underwent a standard cleaning process. To prevent leakage current between the bottom electrode and the substrate, a 500-nm-thick tetraethoxysilane (TEOS) oxide layer was fabricated on the silicon wafer by low-pressure chemical vapor deposition (LPCVD) at 700 °C to act as an insulator. Subsequently, a 200-nm-thick layer of tantalum nitride (TaN) was deposited via reactive sputtering in a 95/5 argon/nitrogen environment. This TaN layer served as the bottom electrode for the resistive memory device. Following this, a 200-nm-thick layer of Ti, used as the displacement material for CDT-Cu, was deposited onto the TaN film by electron beam evaporation.

To perform CDT, the electrolyte was prepared by blending 0.1 M $CuSO_4$ and 0.1 M HF in deionized water with stirring for 20 min until complete dissolution. In this state, various ions, including Cu^{2+}, H^+, and F^+, were released into the electrolyte. To initiate the chemical displacement, samples were immersed in the prepared electrolyte and allowed to sit for a predetermined formation time. In this study, we utilized formation times of 90, 105, and 120 s, which are respectively denoted as CDT-90, CDT-105, and CDT-120 hereafter. For CDT times exceeding 120 s, the surface remained unchanged, signifying the complete displacement and transformation of Ti into a Cu film. During the displacement process, F^+ ions in the electrolyte

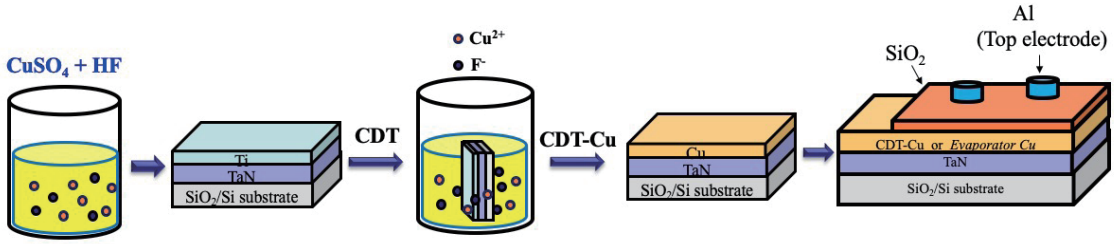

Fig. 1. (Color online) Schematic of fabrication process of CDT-Cu resistive memory device.

interacted with Ti atoms and hence released electrons. The Cu^{2+} ions reacted with these electrons in the electrolyte, leading to a reduction–oxidation reaction, ultimately converting Cu ions into atoms. Consequently, the Ti layer gradually transformed into a Cu film, which became the bottom electrode of the resistive memory device.

Following CDT, the samples were rinsed with deionized water and subjected to a 100 °C curing step for 10 min to remove moisture. A 20-nm-thick SiO_2 film was then deposited on the CDT-Cu electrode to serve as the resistive switching layer of the memory device. Finally, a 100-nm-thick aluminum (Al) film was sputter-deposited on the SiO_2 film to act as the top electrode for the device. Al was selected as the top electrode material owing to its limited diffusion within the oxide film. Consequently, for the operation of the ECM-type ReRAM device, this characteristic ensured that filament formation was primarily governed by the CDT-Cu ions. The Al thin film then underwent lithography and dry etch processes to define the dimensions of the top electrode of the resistive memory device.

As a point of comparison, a control sample with sputtered-Cu as the bottom electrode was also prepared, where all subsequent fabrication steps remain identical to those of the CDT-Cu memory device.

The surface morphology and material compositions of the CDT-Cu sample were analyzed by field-emission scanning electron microscopy (SEM) and energy-dispersive X-ray spectroscopy (EDS), respectively. Surface roughness was observed by atomic force microscopy (AFM). For electrical measurements, a direct current (DC) voltage source was applied to the ReRAM devices. The switching properties of the CDT-Cu ReRAM devices, including the current density versus electrical field (*J*–*E*), current values for devices in the high-resistance state (HRS) and the low-resistance state (LRS), and applied electric fields for sample transforming to LRS/HRS, as well as reliability characteristics including retention and endurance, were assessed using a semiconductor parameter analyzer (Keithley 4200).

3. Results and Discussion

Figure 2(a) presents the SEM image of the sample after 90 s of CDT. The formation of discernible rough film on the surface can be seen. To ascertain the material composition of the film, EDS analysis was conducted. As depicted in Fig. 2(b), the EDS spectrum of the sample

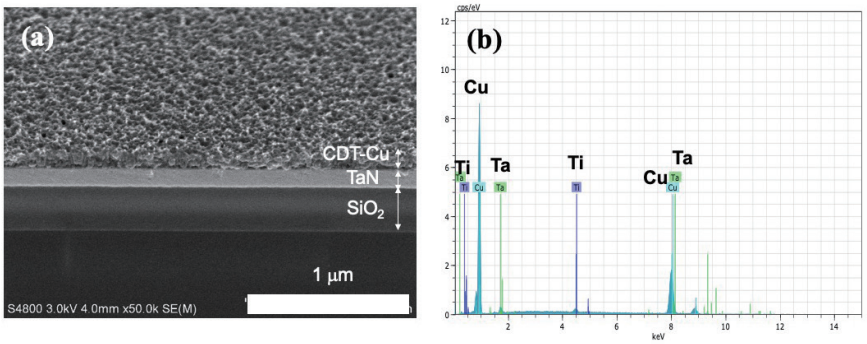

Fig. 2. (Color online) (a) SEM image of the sample after 90 s of CDT. (b) EDS spectrum of Cu grain on the CDT-90 sample.

after 90 s of CDT confirms that the film is predominantly composed of Cu, which constitutes 97% of the weight. The combined SEM and EDS results unequivocally demonstrate the formation of Cu film on the sample surface following the CDT process.

Figure 3 illustrates the *J–E* characteristics of the resistive memory devices under SET and RESET operations. Initially, in the absence of a conductive filament, meaning no pathway existed between the electrodes, the CDT-Cu resistive memory device was in a high-resistance state, commonly referred to as the FRESH state. When a positive voltage was applied to the memory device, Cu atoms on the Cu electrode dissociated into ions, migrated along the direction of the applied electric field, and traveled towards the Al top electrode. Upon reaching the Al electrode, the Cu ions underwent reduction and reverted to atoms.[18] Consequently, a conductive filament formed between the electrodes, resulting in a sharp increase in current, and this current increased up to the compliance of the measuring system, as depicted in the right-hand section of Fig. 3. As a result, the device resistance transitioned from HRS to LRS, marking the successful execution of the SET process. Conversely, applying an effectively negative voltage to an LRS resistive memory device disrupted the existing conductive filament, leading to a significant decrease in current, as evident in the left-hand part of Fig. 3. This action restored the memory device resistance back to a high state and is termed the RESET operation.

Examining the results of *J–E* characteristics, it becomes evident that the electric field of the CDT-Cu memory devices under the SET operation increases with the CDT time. In contrast to the control sample, which had a sputtered-Cu bottom electrode and required a higher electric field for operation, this difference is likely due to the surface roughness of the Cu thin film. To support this inference, we performed AFM measurements of surface roughness. Figure 4 presents AFM images of the CDT-Cu film at various CDT times. The root mean square roughness values are 0.561 nm for the control sample, 2.451 nm for the CDT-90 sample, 5.639 nm for the CDT-105 sample, and 8.373 nm for the CDT-120 sample. These images reveal an overall increase in roughness with longer CDT time. Notably, some obviously bright points are visible in the CDT-90 and CDT-105 images. These points denote sharp Cu grains formed in the

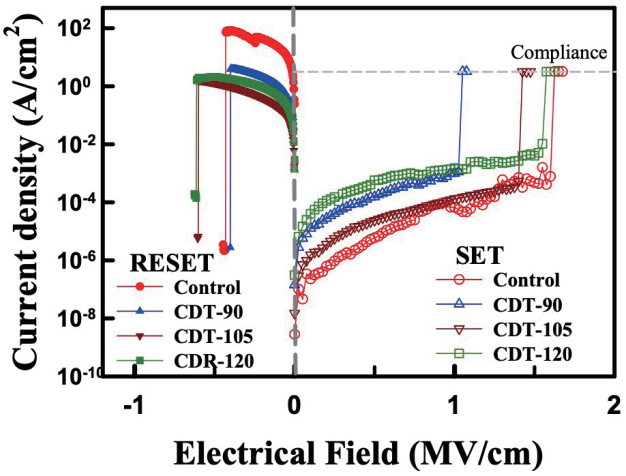

Fig. 3. (Color online) *J–E* characteristics of CDT-Cu resistive memory devices under SET and RESET operations.

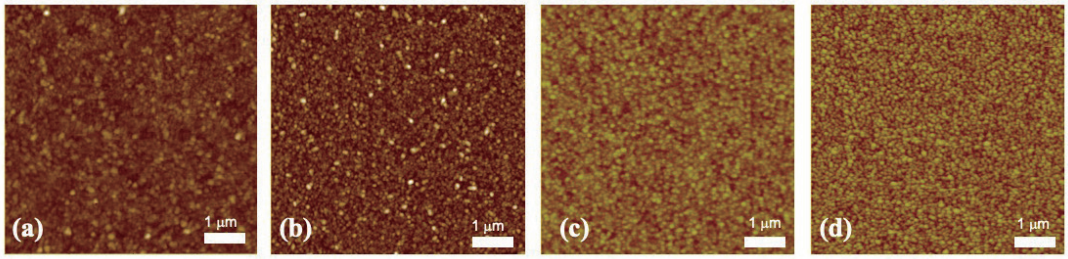

Fig. 4. (Color online) AFM images of CDT-Cu film surface. (a) Control, (b) CDT-90, (c) CDT-105, and (d) CDT-120.

CDT process. The sharp Cu grains possess small radii of curvature, giving rise to a larger local electric field when voltage is applied to the electrode. Because of the corona discharge effect, Cu ions are more readily released from these sharp Cu grains than from other flat surfaces.

Figure 5 displays the electric field distributions for the memory devices under SET and RESET operations. In comparison with the control sample with a sputtered-Cu electrode, the CDT-Cu memory devices exhibit lower and more consistent SET electric fields. This outcome aligns with the findings of the AFM analysis shown in Fig. 4. The Cu thin film produced by the CDT method results in the presence of sharp grains, enhancing the local electric field when voltage is applied. This augmented local field facilitates the diffusion of Cu ions into the SiO_2 thin film, forming the conductive filaments within the resistive switching layer. Consequently, a robust local electric field aids in filament formation and reduces the SET voltage. Moreover, the SET electric field increases as the CDT time increases. These results have a relationship with the diameter of the formed filament, as mentioned in Fig. 3. Attempts were made to reduce the CDT time further to 75 s; however, the results indicated that no copper film was formed on the sample surface. For the RESET operation, a larger electric field is needed for the CDT-120 sample than that for other devices. We inferred that a thicker filament was formed owing to the large grain size of the CDT-120 sample, making it more difficult to rupture the filament. It has been reported that the curvature radius of the grain plays an important role in the local electric field, and therefore the SET/RESET operation is dependent on the grain size by way of the diameter of the forming filament.[19] The schematic representation of the grain size dependence of the formed filament is depicted in Fig. 6.

Figure 7 reveals the cumulative probability of current density for the LRS and HRS CDT-Cu resistive memory devices. It is obvious that the distributions of current density for the LRS devices are larger than those in the case of HRS. No significant distinction is observed between the control and HRS CDT devices. However, the control sample exhibits a higher current density than those of the LRS CDT-Cu devices. Since the current density of the LRS resistive memory device is primarily influenced by the filament diameter, the higher current density in the control sample suggests that a conduction filament with a larger diameter than that in the CDT-Cu devices was formed.

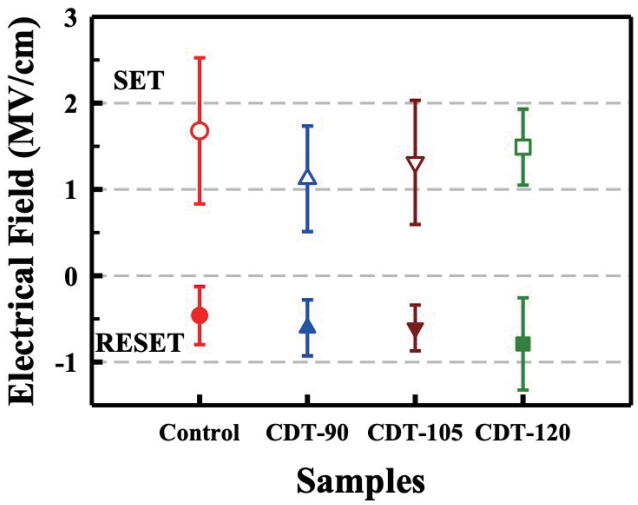

Fig. 5. (Color online) Distributions of electric field for CDT-Cu resistive memory devices under SET and RESET operations.

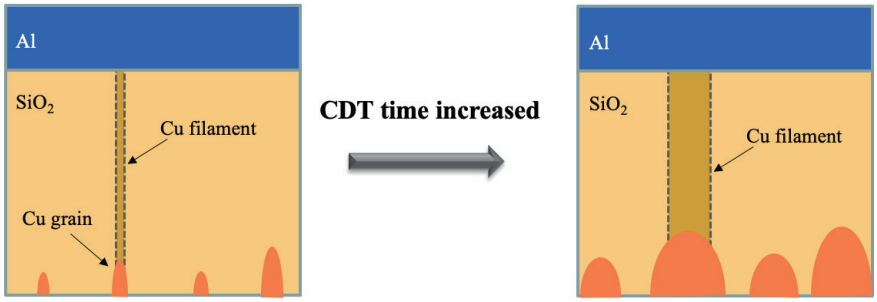

Fig. 6. (Color online) Schematic representation of the Cu grain size dependence of the formed filament.

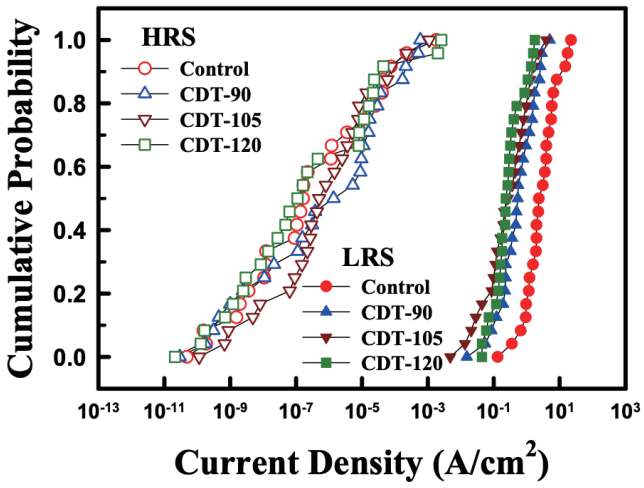

Fig. 7. (Color online) Distributions of LRS and HRS CDT-Cu resistive memory devices. The READ voltage is 0.1 V.

To demonstrate the conduction mechanisms of the CDT-Cu ReRAM devices, the *I–V* characteristic of the LRS and HRS memory devices were measured. Figure 8(a) shows a double logarithmic scale plot of the *J–V* curves for LRS ReRAM devices. The *J–V* curves in Fig. 8(a) display a notable linear relationship, suggesting that electron conduction through the filament follows an ohmic conduction mechanism. Ohmic conduction represents one of the fundamental carrier-conduction mechanisms. This result confirms that the filament is composed of metal, and it can be reasonably inferred that the metal in question is Cu originating from the bottom electrode.

The double-logarithmic-scale *J–E* curve for the HRS CDT-90 ReRAM device is shown in Fig. 8(b). The current exhibits distinct characteristics at different voltages, manifesting three stages with different slopes. In the initial stage under low electric field conditions, the conduction is ohmic, marked by a slope of approximately 1.2. As the electric field intensity increases, the second stage is reached and the slope increases to 2, indicative of the space-charge-limited current (SCLC) effect. Upon prolonged application of the electric field, the conduction enters the third stage, demonstrating trap-filling behavior. In this stage, the slope notably increases to 4.94.

To demonstrate the temperature-dependent memory window of the CDT-Cu ReRAM device, the resistances of LRS and HRS CDT-90 samples were measured at different temperatures. Figure 9 shows the resistances of the CDT-Cu ReRAM device measured at temperatures ranging from 27 to 87 °C. The obtained results confirmed a direct relationship between resistance and measurement temperature. The memory window of the CDT-90 ReRAM device is ~10^6 at 27 °C and decreases to ~10^3 at 87 °C. Notably, it becomes apparent that the resistance in the LRS devices rises with increasing temperature. This observation leads to the inference that the conduction path primarily comprises a metallic conductor, i.e., Cu filament, given its temperature-dependent behavior. Conversely, in the HRS device, resistance decreases as temperature increases, a phenomenon that can be attributed to both the SCLC effect and the diffusion of copper ions under these thermal conditions.

Reliability is also an important feature of the nonvolatile memory device. Figures 10 and 11 show the data retention and endurance characteristics, respectively, of the CDT-Cu ReRAM devices at room temperature. For the retention measurement, a DC sweep was applied to switch

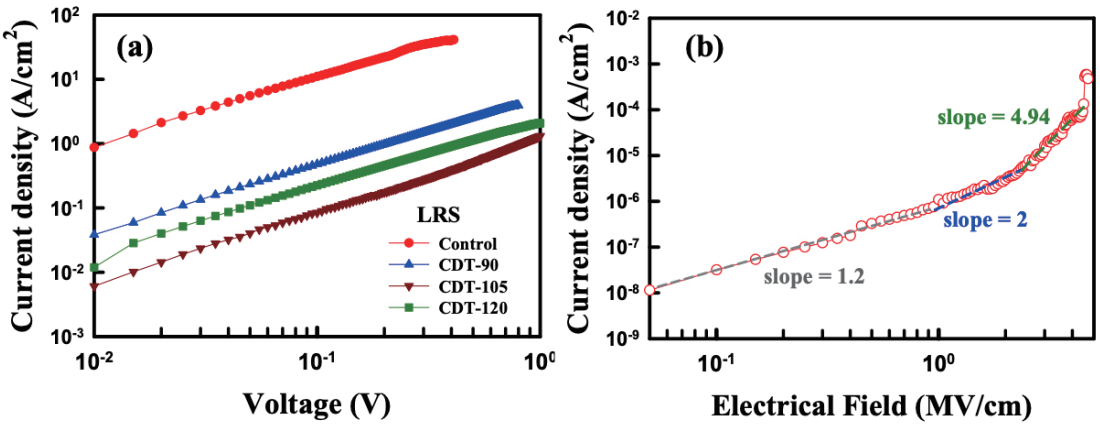

Fig. 8. (Color online) Curve fitting for the LRS and HRS CDT-Cu resistive memory devices. (a) *I–V* curves for the LRS devices. (b) *J–E* curve for the HRS device.

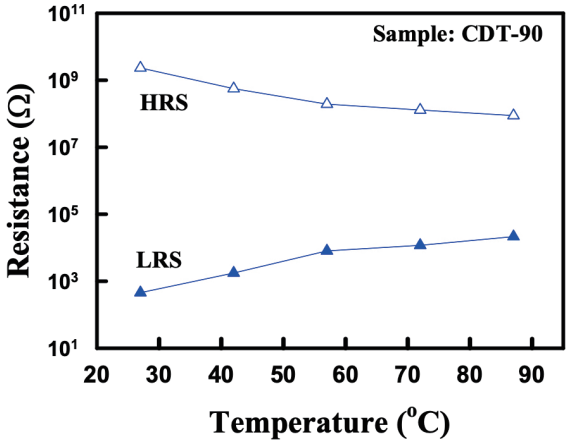

Fig. 9. (Color online) Memory window of the ReRAM device measured at temperatures from room temperature to 87 °C.

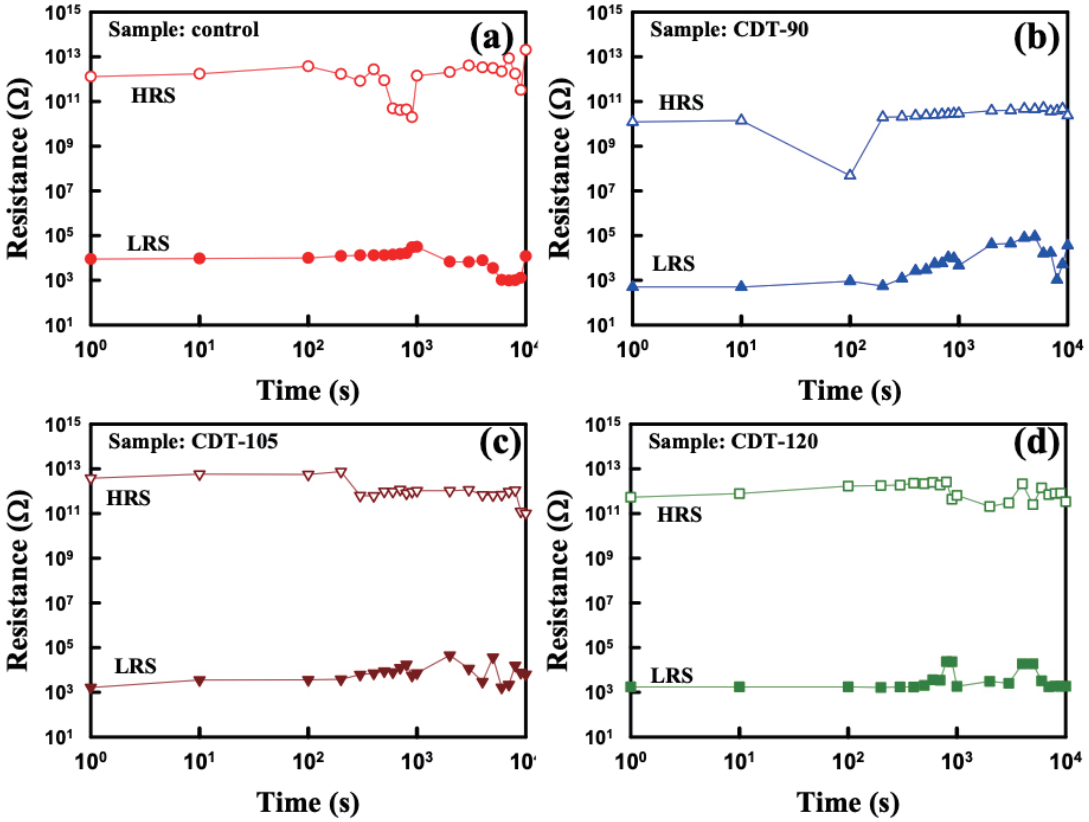

Fig. 10. (Color online) Retention characteristics of ReRAM devices: (a) control, (b) CDT-90, (c) CDT-105, and (d) CDT-120.

the samples between LRS and HRS, with a subsequent application of a voltage of 0.1 V to READ the devices. It was observed that all samples managed to retain data for a duration of 10^4 s with slight window narrowing, and a memory window (R_{HRS}/R_{LRS}) of at least four orders remained after 10^4 s. Moreover, the window of CDT-105 devices reached up to 10^{10}.

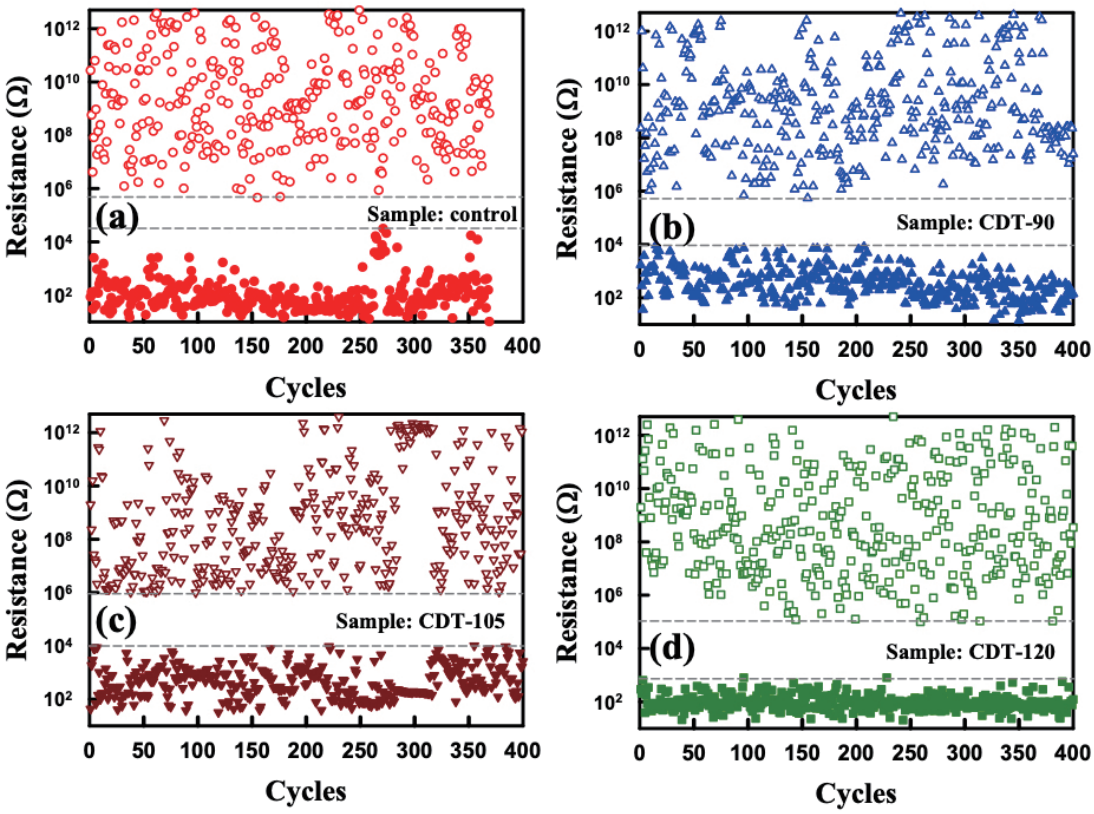

Fig. 11. (Color online) Endurance characteristics of the ReRAM devices: (a) control, (b) CDT-90, (c) CDT-105, and (d) CDT-120.

Figure 11 shows the endurance characteristics of the CDT-Cu ReRAM devices. To evaluate their endurance, a DC sweep cycle was executed, and a voltage of 0.1 V was applied to READ the devices. It can be seen that the copper electrode prepared by CDT can be operated up to 400 times, whereas the sputter-Cu control sample could only be operated 360 times. The better endurance of the CDT-Cu samples than the control device is due to the Joule heating effect. Joule heat was generated during repeated writing and erasing operations, causing the resistance conversion layer to be damaged. CDT-Cu samples possess a lower operating electric field, making the Joule heating effect smaller than that of the control sample.

4. Conclusions

This study involved the fabrication of an electrochemical-migration-type ReRAM device. In this device, a Cu thin film was formed by replacing a Ti film through a straightforward CDT process. The inherent rough surface of the CDT-Cu film contributed to an enhanced local electric field, primarily due to the presence of small Cu grains on the CDT-Cu surface. The results of SEM observation and EDS analysis confirmed the existence of the formed Cu film. AFM images revealed the presence of sharp Cu grains, particularly in samples subjected to a short CDT time. This led to a decrease in the electric field during the SET operation of the

ReRAM device. Furthermore, the CDT-Cu ReRAM devices displayed lower and more consistent operating electric fields than did their sputtered-Cu counterparts, aligning with the observations from the surface analysis. The *J*–*V* and temperature-dependent resistance measurement results confirmed that the filament was composed of Cu. Moreover, the reliability, including the retention and endurance characteristics, of the CDT-Cu ReRAM devices was also evaluated. The results collectively demonstrate that the fabricated CDT-Cu ReRAM devices exhibited commendable electrical performance and reliability.

References

1 M. Nakano, Y. Kaneda, S. Nakanishi, Y. Murai, Y. Tashiro, Y. Taito, T. Ogawa, H. Mitani, T. Ito, and T. Kono: IEEE J. Solid-State Circuits **57** (2022) 3094. http://doi.org/10.1109/Jssc.2022.3168069
2 Y. Baek, B. Bae, J. Y. Yang, D. Lee, H. S. Lee, M. Park, T. Kim, S. Kim, B. I. Park, G. Yoo, and K. S. Lee: Adv. Electron. Mater. **9** (2023) 2300303. http://doi.org/10.1002/aelm.202300303
3 C. C. Sun and D. Q. V. Hoang: Sens. Mater. **34** (2022) 1297. http://doi.org/10.18494/Sam3505
4 Y. Li, Z. C. Zhang, J. Q. Li, X. D. Chen, Y. Kong, F. D. Wang, G. X. Zhang, T. B. Lu, and J. Zhang: Nat. Commun. **13** (2022) 4591. http://doi.org/10.1038/s41467-022-32380-3
5 G. Kim, S. Lee, T. Eom, T. Kim, M. Jung, H. Shin, Y. Jeong, M. Kang, and S. Jeon: J. Mater. Chem. C **10** (2022) 9802. http://doi.org/10.1039/d2tc01608g
6 H. Zhang, L. Liu, D. Wang, H. Lin, X. F. Zhao, and C. Q. Xie: IEEE Trans. Electron. Devices **70** (2023) 4150. https://doi.org/10.1109/TED.2023.3288496
7 S.-H. Liu, C.-C. Wu, W.-L. Yang, Y.-H. Lin, and T.-S. Chao: IEEE Trans. Electron. Devices **61** (2014) 3179. https://doi.org/10.1109/TED.2014.2341629
8 Y. F. Hu, M. Rabelo, T. Kim, J. Cho, J. Choi, X. Y. Fan, and J. S. Yi: Trans. Electr. Electron. Mater. **24** (2023) 271. https://doi.org/10.1007/s42341-023-00445-9
9 B. Fontaine, C. Boixaderas, J. Dubois, P. Gouraud, A. Rival, and N. Posseme: J. Vac. Sci. Technol., A **41** (2023) 053005. https://doi.org/10.1116/6.0002751
10 L. Sun, L. Guo, G. C. Wang, H. Su, B. Liu, and X. L. Tang: Appl. Phys. Lett. **123** (2023) 033502. https://doi.org/10.1063/5.0153972
11 C.-C. Wu, W.-F. Wu, G.-W. Lin, and W.-L. Yang: IEEE Trans. Electron. Devices **67** (2020) 277. https://doi.org/10.1109/ted.2019.2952361
12 S.-H. Liu, W.-L. Yang, C.-C. Wu, T.-S. Chao, M.-R. Ye, Y.-Y. Su, P.-Y. Wang, and M.-J. Tsai: IEEE Electron. Device Lett. **34** (2013) 123. https://doi.org/10.1109/led.2012.2224633
13 C. C. Wu, T. C. Chen, and W. L. Yang: Appl. Phys. Lett. **121** (2022) 213301. https://doi.org/10.1063/5.0127937
14 G. Tarsoly, J. Y. Lee, F. Shan, and S. J. Kim: Appl. Surf. Sci. **601** (2022) 154281. https://doi.org/10.1016/j.apsusc.2022.154281
15 Z. Q. Gao, L. L. Xu, X. Y. Jiao, X. Li, C. J. He, H. Z. Wang, C. Y. Sun, P. X. Hou, C. Liu, and H. M. Cheng: ACS Nano **17** (2023) 18290. https://doi.org/10.1021/acsnano.3c05374
16 S. C. Chen and I. Valov: Adv. Mater. **34** (2022) 2105022. https://doi.org/10.1002/adma.202105022
17 C.-E. Lin, B.-Q. Yu, H.-C. You, Y.-C. Cheng, J.-C. Lin, and C.-C. Wu: Proc. 2023 6th Int. Symp. Computer, Consumer and Control (IEEE, 2023) 230−233. https://doi.org/10.1109/IS3C57901.2023.00068
18 C. C. Wu, H. C. You, Y. H. Lin, C. J. Yang, Y. P. Hsiao, T. P. Liao, and W. L. Yang: Materials **11** (2018) 265. https://doi.org/10.3390/ma11020265
19 P. Zhang, Y. Y. Lau, and R. M. Gilgenbach: J. Appl. Phys. **105** (2009) 114908. https://doi.org/10.1063/1.3131844